The Astrophysical Journal Letters, 886:L10 (7pp), 2019 November 20 https://doi.org/10.3847/2041-8213/ab53e8

Rovibrational Spectral Analysis of CO_3 and C_2O_3: Potential Sources for O_2 Observed in Comet 67P/Churyumov–Gerasimenko

Ryan C. Fortenberry[1], Daniel Peters[1], Brian C. Ferrari[2], and Christopher J. Bennett[2]
[1] Department of Chemistry & Biochemistry, University of Mississippi, University, MS 38677-1848, USA; r410@olemiss.edu
[2] Department of Physics, University of Central Florida, Orlando, FL 32816, USA
Received 2019 August 5; revised 2019 October 26; accepted 2019 November 4; published 2019 November 15

Abstract

The recent *ROSETTA* mission to comet 67P/Churyumov–Gerasimenko detected surprisingly high levels of molecular oxygen (O_2; hypervolatile species) in the coma. Current models predict that considerable levels of other hypervolatiles (such as molecular nitrogen, N_2, methane, CH_4, and Argon) should be found at similar levels, whereas they are more depleted. One explanation explored here is that larger (less volatile) parent molecules may have been formed during radiolysis of cometary ices and, upon sublimation, are subsequently broken down within the coma into smaller, more volatile fragments. In support of this hypothesis, this work employs reliable quantum chemical techniques to provide the spectral data necessary for the detection of two candidate precursor "parent" molecules, cyclic carbon trioxide (c-CO_3), and cyclic dicarbon trioxide (c-C_2O_3). Benchmark computations performed for gas-phase CO_2 give vibrational frequencies to within 1.5 cm^{-1} or better for the three fundamentals. Both c-CO_3 and c-C_2O_3 have strong infrared features in the 4.5–5.5 μm (1800–2200 cm^{-1}) range and other notable infrared features closer to 1100 cm^{-1} (9.10 μm). These molecules are both rotationally active, unlike CO_2, and are therefore potentially observable and present new targets for radio telescope observations. Due to the stronger dipole moment, c-CO_3 should be more easily detectable than the nearly non-polar c-C_2O_3. These data may help observations of these molecules and can provide insights as to how radiation-driven derivatization of CO/CO_2 precursors could contribute to the generation of higher-mass parent species that subsequently degrade to produce more volatile species, such as O_2, observed in cometary comae.

Unified Astronomy Thesaurus concepts: Astrochemistry (75); Molecular spectroscopy (2095); Comets (280)

1. Introduction

In 2015 abundant molecular oxygen was discovered in comet 67P/Churyumov–Gerasimenko (hereafter, 67P) during the *Rosetta* mission (Bieler et al. 2015). Speculation as to the origins of this material vary since most of the O_2 known to exist in the Earths atmosphere is believed to be of biological provenance, which cannot be the case in the interplanetary medium. Prior to encounter, chemical models (Glinski et al. 2004; Pierce & A'Hearn 2010) predicted that some O_2 could be formed in the comae of comets, but not to the levels detected by *Rosetta*. The observations, and several suggested mechanisms for O_2 production in comet 67P, have been reviewed recently (Luspay-Kuti et al. 2018; Altwegg et al. 2019). Several authors have suggested that the O_2 detected could be primordial to the solar system and is being released as molecular O_2 as the comet approaches perihelion. However, many of these models require adoption of specific parameters to favor O_2 production (e.g., higher densities, higher temperatures, higher galactic cosmic radiation rates), while hindering the production of other species, such as ozone, O_3, hydrogen dioxide, HO_2, and hydrogen peroxide, H_2O_2 (Taquet et al. 2016; Heritier et al. 2018; Laufer et al. 2018; Eistrup & Walsh 2019). However, under these considerations, the simultaneous preservation of primordial O_2 alongside the depletion of other hypervolatile species, such as molecular nitrogen, N_2, methane, CH_4, and argon remains challenging to explain since mechanisms such as selective trapping or clathrate formation are unlikely.

Other explanations are more focused on ways to form O_2 at a later stage, or in situ within the coma. The formation of O_2 from the dismutation of H_2O_2 has also been suggested (Dulieu et al. 2017), but the required levels of H_2O_2 needed to explain the formation of O_2 by this mechanism are several orders higher than those observed in 67P. Others have suggested that O_2 forms from interactions of water pick-up ions with the oxidized surface of the rock substrate or grains subsumed in the icy mantle (Yao & Giapis 2017) where energetic O_2^- anions would be the primary product released. Consequently, doubt that such species could be produced in enough abundance to generate the amounts of O_2 in question, as well as whether energetic O_2^- anions would have been detectable, have been raised (Heritier et al. 2018). Furthermore, another intermediate in this surface-catalyzed reaction is the so-called "oxywater" molecule ($H_2O{-}O$), but the stability of this neutral species has been questioned for some time (Meredith et al. 1992; Xie et al. 1996; Franz et al. 2009). Differently, the oxywater cation (H_2OO^+) has been proposed as the progenitor of the O−O bond through reaction of water cations with atomic oxygen leading to an electronically excited state favoring creation of O_2^+ and H_2 (Fortenberry et al. 2019). This reaction has only been proposed theoretically, and likely low abundances of H_2O^+ in 67P may hinder such a process (Fuselier et al. 2016). The potential build-up of O_2 from irradiated water ices has been suggested (Mousis et al. 2018), but the radiolytic yields of O_2 production within pure water are too low to explain the observations (Zheng et al. 2006). Due to these considerations, it may be more likely that the irradiation of other ices besides H_2O could play important roles. For example, the production of O_2 within carbon dioxide (CO_2) ices is often considerably higher (Martín-Doménech et al. 2015), and this ice can be present at levels up to 20% in comets. However, the observations at 67P were consistent with the interpretation that the O_2 signal appears to be correlated with the release of H_2O (Altwegg et al. 2019).

An alternative view of what is occurring is that what is being observed as O_2 by the mass spectrometer may not likely start out as O_2. Instead, it is conceivable that larger, less volatile "parent" species that are produced during the radiolysis of ices are sublimating alongside the H_2O molecules—since they have similar volatility to water—and are then being subsequently degraded. The breakdown of these molecules may occur because these species are unstable in the gas-phase, or due to processes occurring within the cometary coma or within the mass spectrometer. The breakdown of large molecular species has been suggested to account for distributed sources, observed for several molecules (Cottin & Fray 2008). In fact, carbon oxide species, such as carbon suboxide (C_2O_3), have been suggested to account for distributed sources of CO and dicarbon monoxide (C_2O) (Huntress et al. 1991; Bennett et al. 2008), for example.

Here, the potential contribution of larger carbon oxide species produced during the radiolysis of CO_2 ices are investigated to see if they may then sublimate later (i.e., alongside water) and then could potentially contribute to the observed O_2 signal at comet 67P as they are broken down. The simplest such molecule beyond CO_2 itself is carbon trioxide, CO_3. The most stable form is the cyclic C_{2v} molecule, which also happens to be the most abundant form observed produced during the radiolysis of CO_2 ices by ultraviolet (UV) photons (Moll et al. 1966; Gerakines et al. 1996; Martín-Doménech et al. 2015; Radhakrishnan et al. 2018), energetic electrons (e.g., Bennett et al. 2004), and energetic ions (Bennett et al. 2014, and references therein). The less abundant D_{3h} isomer of carbon trioxide has been identified (Jamieson et al. 2006), along with the C_{2v} form of carbon tetraoxide (CO_4; Jamieson et al. 2007b), the C_2 form of carbon pentaoxide (CO_5; Jamieson et al. 2007a), and the C_s form of carbon hexaoxide (CO_6; Jamieson et al. 2008) alongside CO, O_2, and ozone (O_3). Note that although CO_3 is one of the most abundant species formed within these ices, the CO_3^+ (with a mass-to-charge ratio, $m/z = 60$) ion is not typically identified by mass spectrometry during sublimation of irradiated CO_2 ices in these laboratory investigations. This indicates that CO_3 likely dissociates either directly upon sublimation or perhaps it fragments easily when subjected to UV photons or energetic electrons present in the cometary comae; in either case, abundant O_2 and CO (or CO_2 and O) could be produced. Additionally, a $m/z = 60$ peak in the *Rosetta* data is currently attributed to OCS with a mass of 59.966985 amu. CO_3 has a mass of 59.984745 amu (Altwegg & Team 2018), making their difference right at the limit of what is discernable giving some evidence that CO_3 may be present in 67P or similar comets.

Another relatively simple molecule that could sublime from an irradiated CO_2 surface is oxalic anhydride, C_2O_3. This molecule has been suggested to be formed when CO is exposed to high pressures, alongside carbon suboxide (C_3O_2; Lipp et al. 1998), which has been suggested as a parent molecular species that could potentially contribute to the extended source of CO as well as dicarbon (C_2) and dicarbon monoxide (C_2O; Huntress et al. 1991; Bennett et al. 2008). The C_2O_3 molecule is investigated here since it has not been well characterized previously but could potentially be produced during CO_2 irradiation experiments, as evidenced by its infrared absorption bands derived here. This molecule is roughly triangular of C_{2v} symmetry as shown in Figure 1 and is of the same connectivity as the closely related $NCNCN^-$ molecule recently studied (Dubois et al. 2019). Relatively little is known about this molecule, but the proximity of the two outlying oxygen atoms makes them prime targets for gas-phase collisional reactions with other, exposed oxygen species. Such reactions, again, would lead to additional O_2 (and more CO/CO_2).

In any case, CO_3 and C_2O_3 likely dissociate either at or shortly after sublimation and will have short lifetimes in situ making their abundances consistent with the amount of volatiles observed correlating to O_2 (Altwegg & Team 2018). Consequently, if these molecules are to be considered as possible intermediates in the formation of molecular oxygen from carbon dioxide ices, they must be detected in the gas-phase in the laboratory and then in comae in situ. This work is relying upon trusted quantum chemical approaches to provide spectral data for these small, CO_2 derivatives. The expectation is that the data produced herein could serve as guides for the exploration that lower volatility radiation products produced primarily from CO_2 radiolysis could be contributing to the detected O_2 yield.

2. Computational Details

Coupled cluster theory at the singles, doubles, and perturbative triples level (Raghavachari et al. 1989) within the F12 explicitly correlated electron formalism (Adler et al. 2007; Knizia et al. 2009) and a triple-zeta basis set (Hill & Peterson 2010) is employed. Then, these CCSD(T)-F12b/cc-pVTZ-F12 (hereafter, F12-TZ) energies are utilized within a fourth-order Taylor series expansion of the internuclear Hamiltonian's potential (or quartic force field (QFF)) to produce the spectroscopic data. Such an approach has been shown previously to match higher-level computations exceptionally well (Agbaglo et al. 2019; Agbaglo & Fortenberry 2019a, 2019b) including $NCNCN^-$ (Dubois et al. 2019). Similar computational analysis has also preceded subsequent experimental and astronomical detection of various molecules (Huang et al. 2011; Fortenberry et al. 2012; Zhao et al. 2014; Theis & Fortenberry 2016; Bizzocchi et al. 2017; Fortenberry & Francisco 2017; Fuente et al. 2017; Wagner et al. 2018).

The QFFs begin with geometry optimizations of each molecule with the F12-TZ approach. Then, energy points are created with displacements of ± 0.005 Å for bond lengths and ± 0.005 radians from this reference geometry in order to compute the numerical derivatives up to fourth-order. At each point, the F12-TZ energies are computed. All F12-TZ computations use the MOLPRO 2015.1 quantum chemical program (Werner et al. 2012, 2015). A least-squares fit produces the equilibrium geometry, and a refit produces the necessary force constants. The INTDER program (Allen et al. 2005) transforms the symmetry-internal coordinates for each molecule (defined below) into Cartesian coordinates for generic use within the SPECTRO program (Gaw et al. 1991). Second-order rotational (Mills 1972) and vibrational perturbation theory (VPT2; Watson 1977; Papousek & Aliev 1982) are utilized therein to produce the spectroscopic constants and vibrational frequencies.

CO_2 is exhibiting the known $2\nu_3 = \nu_2$ type-1 Fermi resonance which is accounted for in the VPT2 computations within SPECTRO. CO_3 has a $2\nu_3 = 2\nu_2 = \nu_1$ Fermi resonance polyad, as well as a $2\nu_5 = \nu_2$ type-1 Fermi resonance and a $\nu_6 + \nu_5 = \nu_3$ type-2 Fermi resonance. ν_6/ν_5 C-type and

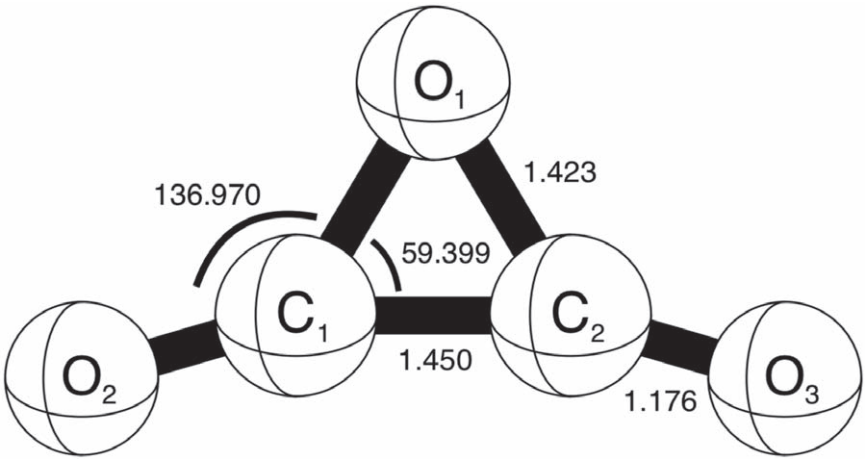

Figure 1. CCSD(T)-F12/cc-pVTZ-F12 equilibrium geometry (in Å and °) of $^1A_1$ C_2O_3.

ν_6/ν_4 A-type Coriolis resonances are also present. C_2O_3 possesses $2\nu_3 = \nu_4 + \nu_3 = \nu_7 + \nu_2 = \nu_1$, $2\nu_5 = \nu_7 + \nu_6 = \nu_9 + \nu_4 = \nu_3$; and $2\nu_7 = 2\nu_8 = \nu_4$ Fermi resonance polyads. It further has $\nu_6 + \nu_3 = \nu_2$, $\nu_8 + \nu_7 = \nu_5$, and $\nu_9 + \nu_7 = \nu_6$ type-2 Fermi resonances as well as ν_6/ν_5 A-type, ν_9/ν_7 C-type, and ν_9/ν_8 A-type Coriolis resonances. The intensities are computed with MP2/6-31 + G* in the Gaussian09 program (Møller & Plesset 1934; Hehre et al. 1972; Frisch et al. 2009) shown previously to give good results compared to higher-order computations (Yu et al. 2015; Finney et al. 2016).

The symmetry-internal coordinates for CO_2 are simply: (1) the C=O symmetric stretch, (2) the C=O antisymmetric stretch, and 3/4) the bend(s). The symmetry-internal coordinates for CO_3 are below with atoms numbered relative to Figure 2 with OPB is defined as the out-of-plane bend:

$$S_1(a_1) = \mathrm{C} - \mathrm{O}_1 \tag{1}$$

$$S_2(a_1) = \frac{1}{\sqrt{2}}[(\mathrm{O}_2 - \mathrm{C}) + (\mathrm{O}_3 - \mathrm{C})] \tag{2}$$

$$S_3(a_1) = \frac{1}{\sqrt{2}}[\angle(\mathrm{O}_2 - \mathrm{C} - \mathrm{O}_1) + \angle(\mathrm{O}_3 - \mathrm{C} - \mathrm{O}_1)] \tag{3}$$

$$S_4(b_2) = \frac{1}{\sqrt{2}}[(\mathrm{O}_2 - \mathrm{C}) - (\mathrm{O}_3 - \mathrm{C})] \tag{4}$$

$$S_5(b_2) = \frac{1}{\sqrt{2}}[\angle(\mathrm{O}_2 - \mathrm{C} - \mathrm{O}_1) - \angle(\mathrm{O}_3 - \mathrm{C} - \mathrm{O}_1)] \tag{5}$$

$$S_6(b_1) = OPB(\mathrm{O}_1 - \mathrm{C} - \mathrm{O}_2 - \mathrm{O}_3). \tag{6}$$

The symmetry-internal coordinates for C_2O_3 with atoms numbered relative to Figure 1 are given as

$$S_1(a_1) = \mathrm{C}_1 - \mathrm{C}_2 \tag{7}$$

$$S_2(a_1) = \frac{1}{\sqrt{2}}[(\mathrm{O}_1 - \mathrm{C}_1) + (\mathrm{O}_1 - \mathrm{C}_2)] \tag{8}$$

$$S_3(a_1) = \frac{1}{\sqrt{2}}[(\mathrm{C}_1 - \mathrm{O}_2) + (\mathrm{C}_2 - \mathrm{O}_3)] \tag{9}$$

$$S_4(a_1) = \frac{1}{\sqrt{2}}[\angle(\mathrm{O}_2 - \mathrm{C}_1 - \mathrm{O}_1) + \angle(\mathrm{O}_3 - \mathrm{C}_2 - \mathrm{O}_1)] \tag{10}$$

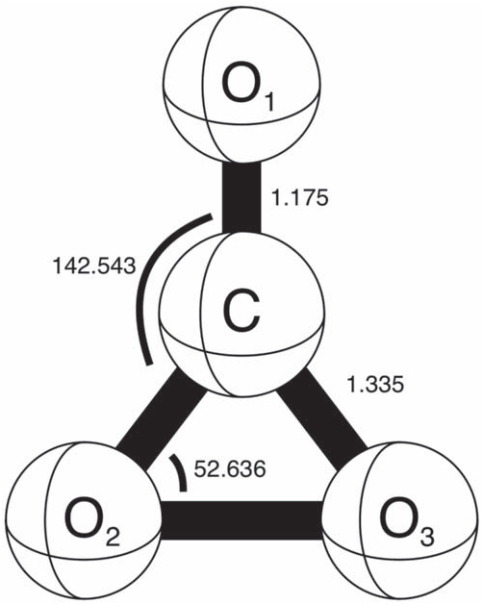

Figure 2. CCSD(T)-F12/cc-pVTZ-F12 equilibrium geometry (in Å and °) of $^1A_1$ CO_3.

$$S_5(b_2) = \frac{1}{\sqrt{2}}[(\mathrm{O}_1 - \mathrm{C}_1) - (\mathrm{O}_1 - \mathrm{C}_2)] \tag{11}$$

$$S_6(b_2) = \frac{1}{\sqrt{2}}[(\mathrm{C}_1 - \mathrm{O}_2) - (\mathrm{C}_2 - \mathrm{O}_3)] \tag{12}$$

$$S_7(b_2) = \frac{1}{\sqrt{2}}[\angle(\mathrm{O}_2 - \mathrm{C}_1 - \mathrm{O}_1) - \angle(\mathrm{O}_3 - \mathrm{C}_2 - \mathrm{O}_1)] \tag{13}$$

$$S_8(b_1) = \frac{1}{\sqrt{2}}[\tau(\mathrm{O}_2 - \mathrm{C}_1 - \mathrm{O}_1 - \mathrm{C}_2) - \tau(\mathrm{O}_3 - \mathrm{C}_2 - \mathrm{O}_1 - \mathrm{C}_1)] \tag{14}$$

$$S_9(a_2) = \frac{1}{\sqrt{2}}[\tau(\mathrm{O}_2 - \mathrm{C}_1 - \mathrm{O}_1 - \mathrm{C}_2) + \tau(\mathrm{O}_3 - \mathrm{C}_2 - \mathrm{O}_1 - \mathrm{C}_1)] \tag{15}$$

where τ represents the torsion/dihedral angle for the subsequent four atoms. This type of treatment has proven

Table 1
CCSD(T)-F12/cc-pVTZ-F12 Harmonic and Anharmonic (QFF) Rotational Constants (MHz), Dipole Moments (D), and Vibrational Frequencies (cm^{-1}) with Intensities in Parentheses (km/mol) with Frequency Ordering from Highest to Lowest

	CO_2			CO_3			C_2O_3	
	Symmetry	Present Work	Experiment[a]	Symmetry	Present Work (C_{2v})	Experiment[b]	Symmetry	Present Work
A_0					24064.6			19178.8
B_0		11658.8	11698		9343.4			4157.6
C_0					6715.9			3412.4
A_e					24242.7			19375.9
B_e		11700.1			9367.2			4165.8
C_e					6756.5			3428.7
D_J (kHz)[c]		3.894	3.9973727		2.714			0.569
D_{JK} (kHz)					24.126			−1.746
D_K (kHz)					102.356			154.696
H_J (mHz)[c]		0.338	0.23084		0.003			0.001
H_{JK} (mHz)					−0.154			0.010
H_{KJ} (mHz)					1.072			−0.631
H_K (mHz)					−1.124			3.826
μ		…	…		0.70			0.09
ω_1	σ_u	2395.0 (566)	(665)	a_1	2055.6 (540)		a_1	2124.5 (124)
ω_2	σ_g	1353.0 (0)	(0)	a_1	1092.1 (15)		b_2	1868.0 (581)
ω_3	π_u	673.0 (26)	(54)	b_2	993.2 (187)		a_1	1148.4 (164)
ω_4				b_1	673.8 (29)		a_1	854.6 (1)
ω_5				a_1	609.3 (18)		b_2	662.9 (28)
ω_6				b_2	569.1 (8)		a_2	645.6 (0)
ω_7							b_1	436.3 (31)
ω_8							b_2	343.1 (147)
ω_9							a_1	342.6 (2)
ν_1	σ_u	2348.6	2349	a_1	2055.6	2045	a_1	2084.4
ν_2	σ_g	1332.5	1333	a_1	1065.1	1068	b_2	1857.8
ν_3	π_u	668.2	667	b_2	965.0	973	a_1	1155.6
ν_4				b_1	666.7		a_1	839.4
ν_5				a_1	686.1		b_2	642.2
ν_6				b_2	563.2	565	a_2	630.5
ν_7							b_1	369.1
ν_8							b_2	339.5
ν_9							a_1	337.2
ZPVE		2536.3			2979.2			4178.1

Notes.
[a] Data from Herzberg (1966), Shimanouchi (1972), Rothman et al. (1992).
[b] Data from Bennett et al. (2004).
[c] For CO_2, these should be understood to be D and H as there is no branching in the linear molecule.

necessary in related systems (Fortenberry et al. 2017; Dubois et al. 2019).

3. Results and Discussion

As shown in Table 1 initial benchmarking with the carbon dioxide molecule is exceptional. The F12-TZ anharmonic vibrational frequencies are within 1.5 cm^{-1} (0.03 μm) or less for each of the three fundamental modes (Shimanouchi 1972) further corroborating the benchmarks for this level of theory with *c*-(C)C_3H_2 and $NCNCN^-$ (Agbaglo et al. 2019 and Dubois et al. 2019). The lower-level, double-harmonic computed intensities are also in semi-quantitative agreement and are certainly in the right proportion with one another. The experimentally inferred rotational constant of 11,698 MHz (Herzberg 1966) is within 40 MHz of the F12-TZ computations. Hence, the F12-TZ QFF results should be able to predict accurately the infrared and millimeter wave properties for observation of these possible CO_2 ice derivatives. It should also be noted that the vibrational modes are ordered by frequency and not by symmetry in Table 1 for more direct comparison between molecules in the present study.

While there is much debate as to the ground state of CO_3, this study will limit itself to the C_{2v} isomer. Part of this is due to convenience for the use of this symmetry and that the present computations put the D_{3h} isomer 0.27 eV higher in energy. Another reason for studying the C_{2v} isomer is the exceptionally bright ν_1 (a_1) intensity for the C=O stretch at the apex of the molecule. This intensity is on the order of that for the antisymmetric stretch in carbon dioxide and will fall close to 2055.6 cm^{-1} (4.86 μm) in a spectral region of many lines but few even qualitative spectral assignments. This mode also exhibits no apparent anharmonicity, but such behavior results simply from proper inclusion of the $2\nu_3 = 2\nu_2 = \nu_1$ Fermi resonance polyad (Martin & Taylor 1997). Additionally, previous experimental work on CO_3 indicates that the frequency at 2045 cm^{-1} (Bennett et al. 2004) is likely caused by the C_{2v} isomer due to the correlation of the experimental and theoretical values here. The antisymmetric ν_3 (b_2) stretch at

Table 2
CCSD(T)-F12/cc-pVTZ-F12 Force Constants for CO_2 and CO_3 and Harmonic Force Constants for C_2O_3 in mdyne/(Å^{n}rad^m)

CO_2		CO_3						C_2O_3	
$F_{44} = F_{33}$	0.786186	F_{11}	15.318271	F_{552}	−0.6972	F_{5411}	2.87	F_{11}	5.193773
F_{22}	14.746201	F_{21}	1.117484	F_{553}	−0.5130	F_{5421}	1.29	F_{21}	−0.011872
F_{11}	17.252686	F_{22}	8.147579	F_{661}	−0.2110	F_{5422}	−0.59	F_{22}	4.159832
$F_{441} = F_{331}$	−1.6586	F_{31}	0.532870	F_{662}	−5.2395	F_{5431}	0.96	F_{31}	0.680483
F_{221}	−78.6236	F_{32}	−2.410035	F_{663}	9.5412	F_{5432}	0.59	F_{32}	0.743305
F_{111}	−86.3217	F_{33}	5.248298	F_{1111}	617.90	F_{5433}	−2.96	F_{33}	15.402199
$F_{4444} = F_{3333}$	1.40	F_{44}	4.399800	F_{2111}	7.04	F_{5444}	3.75	F_{41}	0.006224
F_{4433}	1.52	F_{54}	0.367289	F_{2211}	4.49	F_{5511}	0.89	F_{42}	−0.004906
F_{4422}	−1.94	F_{55}	0.701563	F_{2221}	0.76	F_{5521}	1.87	F_{43}	0.032514
F_{3322}	−1.94	F_{66}	0.779582	F_{2222}	139.50	F_{5522}	0.45	F_{44}	1.423942
F_{2222}	309.19	F_{111}	−107.8444	F_{3111}	0.30	F_{5531}	1.39	F_{55}	1.493720
$F_{4411} = F_{3311}$	2.85	F_{211}	−3.1719	F_{3211}	2.63	F_{5532}	0.48	F_{65}	1.260481
F_{2211}	324.81	F_{221}	−1.3879	F_{3221}	1.99	F_{5533}	−1.38	F_{66}	14.804001
F_{1111}	345.09	F_{222}	−38.2000	F_{3222}	−20.12	F_{5544}	−1.10	F_{75}	0.439303
		F_{311}	−1.2560	F_{3311}	2.33	F_{5554}	0.59	F_{76}	0.207699
		F_{321}	−1.1362	F_{3321}	1.08	F_{5555}	1.12	F_{77}	0.973483
		F_{322}	10.0412	F_{3322}	38.09	F_{6611}	−2.02	F_{88}	0.215159
		F_{331}	−1.4607	F_{3331}	0.47	F_{6621}	−0.51	F_{99}	0.271903
		F_{332}	−20.8658	F_{3332}	−116.79	F_{6622}	18.91		
		F_{333}	56.4557	F_{3333}	362.60	F_{6631}	−1.11		
		F_{441}	−1.1670	F_{4411}	−0.73	F_{6632}	−44.26		
		F_{442}	−26.9634	F_{4421}	3.03	F_{6633}	130.98		
		F_{443}	−4.6166	F_{4422}	118.41	F_{6644}	−6.55		
		F_{541}	−1.1976	F_{4431}	6.26	F_{6654}	0.19		
		F_{542}	−0.2886	F_{4432}	15.83	F_{6655}	2.59		
		F_{543}	−0.6107	F_{4433}	−41.28	F_{6666}	52.16		
		F_{551}	−1.1297	F_{4444}	119.69				

Table 3
CCSD(T)-F12/cc-pVTZ-F12 Cubic and Quartic Force Constants for C_2O_3 in mdyne/(Å^{n}rad^m)

F_{111}	−32.7983	F_{774}	−0.3572	F_{4441}	0.055	F_{7531}	−1.902	F_{8833}	−0.124
F_{211}	0.3568	F_{881}	−0.1369	F_{4442}	1.330	F_{7532}	0.801	F_{8841}	0.050
F_{221}	0.3826	F_{882}	−0.0773	F_{4443}	0.384	F_{7533}	1.823	F_{8842}	−0.134
F_{222}	−17.9154	F_{883}	−0.1862	F_{4444}	1.619	F_{7541}	2.351	F_{8843}	−0.127
F_{311}	−0.6333	F_{884}	0.0813	F_{5511}	4.131	F_{7542}	0.139	F_{8844}	−0.351
F_{321}	−0.1643	F_{985}	−0.1000	F_{5521}	−3.227	F_{7543}	1.589	F_{8855}	0.034
F_{322}	−0.8281	F_{986}	−0.2880	F_{5522}	89.452	F_{7544}	0.376	F_{8865}	0.097
F_{331}	−1.3270	F_{987}	−0.0603	F_{5531}	3.022	F_{7555}	4.633	F_{8866}	0.216
F_{332}	−1.6686	F_{991}	−0.2199	F_{5532}	0.775	F_{7611}	−1.070	F_{8875}	−0.041
F_{333}	−76.3309	F_{992}	−0.1491	F_{5533}	−3.040	F_{7621}	0.330	F_{8876}	0.119
F_{411}	1.2940	F_{993}	−0.2814	F_{5541}	−2.832	F_{7622}	1.130	F_{8877}	−0.151
F_{421}	−0.6045	F_{994}	0.0577	F_{5542}	−0.497	F_{7631}	−2.241	F_{8888}	0.126
F_{422}	−0.2174	F_{1111}	155.728	F_{5543}	1.841	F_{7632}	2.238	F_{9851}	0.301
F_{431}	0.3471	F_{2111}	−0.472	F_{5544}	1.408	F_{7633}	0.260	F_{9852}	0.099
F_{432}	−0.3530	F_{2211}	−4.698	F_{5555}	62.290	F_{7641}	1.590	F_{9853}	0.091
F_{433}	0.0712	F_{2221}	−1.885	F_{6511}	4.688	F_{7642}	0.857	F_{9854}	−0.120
F_{441}	−0.3119	F_{2222}	77.599	F_{6521}	1.695	F_{7643}	0.591	F_{9861}	0.881
F_{442}	−1.0190	F_{3111}	1.875	F_{6522}	−2.941	F_{7644}	0.262	F_{9862}	−0.285
F_{443}	−1.4777	F_{3211}	−0.359	F_{6531}	4.902	F_{7655}	−1.635	F_{9863}	−0.061
F_{444}	−0.4769	F_{3221}	1.190	F_{6532}	0.678	F_{7665}	1.734	F_{9864}	0.156
F_{551}	−1.7783	F_{3222}	−2.278	F_{6533}	2.754	F_{7666}	−0.219	F_{9871}	−0.258
F_{552}	−19.1612	F_{3311}	−1.184	F_{6541}	−2.128	F_{7711}	−0.443	F_{9872}	0.049
F_{553}	1.2862	F_{3321}	1.034	F_{6542}	1.908	F_{7721}	0.790	F_{9873}	0.106
F_{554}	0.1235	F_{3322}	2.272	F_{6543}	0.449	F_{7722}	−0.755	F_{9874}	−0.127
F_{651}	−3.7816	F_{3331}	2.619	F_{6544}	1.984	F_{7731}	1.898	F_{9911}	0.361
F_{652}	0.8059	F_{3332}	2.543	F_{6555}	8.955	F_{7732}	1.069	F_{9921}	−0.163
F_{653}	−2.2368	F_{3333}	308.104	F_{6611}	2.117	F_{7733}	0.249	F_{9922}	−0.276
F_{654}	−0.3358	F_{4111}	0.455	F_{6621}	0.385	F_{7741}	−0.858	F_{9931}	0.634
F_{661}	−1.4016	F_{4211}	−0.269	F_{6622}	1.688	F_{7742}	1.308	F_{9932}	0.062
F_{662}	−1.6577	F_{4221}	−0.363	F_{6631}	1.664	F_{7743}	0.486	F_{9933}	−0.223
F_{663}	−74.9695	F_{4222}	1.464	F_{6632}	2.378	F_{7744}	1.967	F_{9941}	−0.010
F_{664}	−0.0444	F_{4311}	−0.843	F_{6633}	307.763	F_{7755}	−1.076	F_{9942}	0.152

Table 3
(Continued)

F_{751}	1.7670	F_{4321}	0.240	F_{6641}	−1.868	F_{7765}	1.548	F_{9943}	−0.092
F_{752}	−0.6787	F_{4322}	0.917	F_{6642}	1.879	F_{7766}	0.700	F_{9944}	−0.280
F_{753}	−0.7817	F_{4331}	−0.982	F_{6643}	−0.169	F_{7775}	0.435	F_{9955}	0.300
F_{754}	−1.3130	F_{4332}	0.883	F_{6644}	0.391	F_{7776}	0.829	F_{9965}	0.028
F_{761}	1.2312	F_{4333}	−0.425	F_{6655}	−0.421	F_{7777}	1.662	F_{9966}	0.125
F_{762}	−1.1078	F_{4411}	−1.457	F_{6665}	2.637	F_{8811}	0.255	F_{9975}	−0.066
F_{763}	−0.3939	F_{4421}	1.071	F_{6666}	309.821	F_{8821}	−0.231	F_{9976}	0.233
F_{764}	−1.1753	F_{4422}	−0.452	F_{7511}	−2.123	F_{8822}	0.025	F_{9977}	−0.230
F_{771}	−1.2774	F_{4431}	0.457	F_{7521}	−0.475	F_{8831}	0.385	F_{9988}	0.082
F_{772}	−0.5040	F_{4432}	2.082	F_{7522}	1.240	F_{8832}	0.027	F_{9999}	0.256
F_{773}	−0.9564	F_{4433}	0.389						

965.0 cm^{-1} (10.36 μm) is roughly 25% of the intensity of ν_1 implying that it will also create a notable transition in any spectrum and is within 8 cm^{-1} of the attributed peak from the same referenced experiment (Bennett et al. 2004). The other vibrational modes are relatively dim and are shifted toward the far-infrared, but correlation between the present theoretical and previous experimental ν_2 and ν_6 fundamentals are noteworthy differing between the two approaches by less than 3 cm^{-1} in each case. Hence, the previous experimental work on CO_3 is likely for the C_{2v} isomer. Regardless, the 0.70 D dipole moment of CO_3 may also make it detectable with radio telescopes from the ground unlike its linear CO_2 cousin.

The force constants, given in Tables 2 and 3, show that the C=O_1 bond, ordered from Figure 2, at the apex of the molecule (F_{11} at 15.318 mdyne/Å^2) is bonded much more strongly than the two externally, exposed oxygen atoms (O_2 and O_3) at each side (F_{22} 8.148 mydne/Å^2). Hence, the bond order for the apical C=O bond is nearly twice that for the other two C−O indicative of double bonds in the ketone moiety at the apex, and single bonds on the sides. The F_{33} force constant of 5.248 mydne/Å^2 also implies a single O_2−O_3 bond at the bottom of the molecule in Figure 2. In any case, vibrational excitation of the ν_5 (a_1) symmetric bend at 686.1 cm^{-1} (14.58 μm) could further promote bonding between the two symmetric oxygen atoms leading to formation of molecular oxygen and CO.

The C_2O_3 molecule has even more bright infrared fundamental vibrational frequencies. All of the stretches above 1100 cm^{-1} (9.10 μm) have large intensities. Most notably, the 1857.8 cm^{-1} (5.38 μm) ν_2 (b_2) antisymmetric C=O stretch involving the external O_2 and O_3 atoms is, again, on the order of the antisymmetric stretch in carbon dioxide. The two other stretches in this frequency region are once more roughly 25% of this bright mode. However, the ν_8 (b_1) out-of-plane bend at 339.5 cm^{-1} (29.46 μm) also has an intensity of this magnitude. The 0.09 D dipole moment implies that this molecule is also detectable via radio telescopes in theory, but the low value is not as promising for detection as the infrared bands should be.

4. Conclusions

In order to detect either of these molecules as possible precursors to O_2 formation in comet 67P, the spectral data provided here are essential. Furthermore, the previous experimental work on CO_3 gives indication of originating with the C_{2v} isomer. CO_3 and C_2O_3 have bright infrared bands in little-understood regions of the mid-infrared and have detectable dipole moments and corroborate the available experimental data. Additionally, the exposed oxygen atoms in both molecules could be donated to other oxygen atoms creating O_2. CO_3 should do this more readily since O_2 could form directly from this molecule due to the existence of a seeming O−O bond and relatively weak C−O bonds. The external C=O bonds in C_2O_3 are fairly strong, and do not have a corresponding vibrational fundamental leading to O−O bond formation. In any case, the data provided here will allow these novel molecules to be detected either in the laboratory or in cometary environments and could shed light onto the formation of O_2 in comet 67P.

R.C.F. acknowledges funding from NASA grant NNX17AH15G, NSF grant OIA-1757220, and start-up funds provided by the University of Mississippi. C.J.B. acknowledges funding from the NASA Solar System Exploration Research Virtual Institute CLASS (NNA14AB05A).

ORCID iDs

Ryan C. Fortenberry https://orcid.org/0000-0003-4716-8225

References

Adler, T. B., Knizia, G., & Werner, H.-J. 2007, JChPh, 127, 221106
Agbaglo, D., & Fortenberry, R. C. 2019a, IJQC, 119, e25899
Agbaglo, D., & Fortenberry, R. C. 2019b, CPL, 734, 136720
Agbaglo, D., Lee, T. J., Thackston, R., & Fortenberry, R. C. 2019, ApJ, 871, 236
Allen, W. D., et al. 2005, INTDER 2005: General Program, Which Performs Vibrational Analysis and Higher-Order Non-Linear Transformations
Altwegg, K., Balsiger, H., & Fuselier, S. A. 2019, ARA&A, 57, 113
Altwegg, K. & Team, R. 2018, in IAU Symp. 332, Astrochemistry VII: Through the Cosmos from Galaxies to Planets, ed. M. Cunningham, T. Millar, & Y. Aikawa (Cambridge: Cambridge Univ. Press), 153
Bennett, C. J., Ennis, C. P., & Kaiser, R. I. 2014, ApJ, 794, 57
Bennett, C. J., Jamieson, C., Mebel, A. M., & Kaiser, R. I. 2004, PCCP, 6, 735
Bennett, C. J., Jamieson, C. S., & Kaiser, R. I. 2008, P&SS, 56, 1181
Bieler, A., Altwegg, K., Balsiger, H., et al. 2015, Natur, 526, 678
Bizzocchi, L., Lattanzi, V., Laas, J., et al. 2017, A&A, 602, A34
Cottin, H., & Fray, N. 2008, SSRv, 138, 179
Dubois, D., Sciamma-O'Brien, E., & Fortenberry, R. C. 2019, ApJ, 883, 109
Dulieu, F., Minissale, M., & Bockelée-Morvan, D. 2017, A&A, 597, A56
Eistrup, C., & Walsh, C. 2019, A&A, 621, A75
Finney, B., Fortenberry, R. C., Francisco, J. S., & Peterson, K. A. 2016, JChPh, 145, 124311
Fortenberry, R. C., & Francisco, J. S. 2017, ApJ, 835, 243
Fortenberry, R. C., Huang, X., Francisco, J. S., Crawford, T. D., & Lee, T. J. 2012, JChPh, 136, 234309
Fortenberry, R. C., Lee, T. J., & Layfield, J. P. 2017, JChPh, 147, 221101
Fortenberry, R. C., Trabelsi, T., Westbrook, B. R., Del Rio, W. A., & Francisco, J. S. 2019, JChPh, 150, 201103
Franz, J., Francisco, J. S., & Peyerimhoff, S. D. 2009, JChPh, 130, 084304
Frisch, M. J., Trucks, G. W., Schlegel, H. B., et al. 2009, Gaussian 09 Revision D.01 (Wallingford, CT: Gaussian, Inc.)
Fuente, A., Goicoechea, J. R., Pety, J., et al. 2017, ApJL, 851, 49

Fuselier, S., Altwegg, K., Balsiger, H., et al. 2016, MNRAS, 462, S67
Gaw, J. F., Willets, A., Green, W. H., & Handy, N. C. 1991, in Advances in Molecular Vibrations and Collision Dynamics, ed. J. M. Bowman & M. A. Ratner (Greenwich, CT: JAI Press, Inc.), 170
Gerakines, P., Schutte, W., & Ehrenfreund, P. 1996, A&A, 312, 289
Glinski, R. J., Ford, B. J., Harris, W. M., Anderson, C. M., & Morgenthaler, J. P. 2004, ApJ, 608, 601
Hehre, W. J., Ditchfeld, R., & Pople, J. A. 1972, JChPh, 56, 2257
Heritier, K. L., Altwegg, K., Berthelier, J.-J., et al. 2018, NatCo, 9, 2580
Herzberg, G. 1966, Electronic Spectra and Electronic Structure of Polyatomic Molecules (New York: Van Nostrand)
Hill, J. G., & Peterson, K. A. 2010, PCCP, 12, 10460
Huang, X., Taylor, P. R., & Lee, T. J. 2011, JPCA, 115, 5005
Huntress, W., Jr, Alien, M., & Delrtsky, M. 1991, Natur, 352, 316
Jamieson, C. S., Mebel, A. M., & Kaiser, R. I. 2006, Chem. Phys. Chem., 7, 2508
Jamieson, C. S., Mebel, A. M., & Kaiser, R. I. 2007a, CPL, 443, 49
Jamieson, C. S., Mebel, A. M., & Kaiser, R. I. 2007b, CPL, 440, 105
Jamieson, C. S., Mebel, A. M., & Kaiser, R. I. 2008, CPL, 450, 312
Knizia, G., Adler, T. B., & Werner, H.-J. 2009, JChPh, 130, 054104
Laufer, D., Bar-Nun, A., & Ninio Greenberg, A. 2018, MNRAS, 469, S818
Lipp, M., Evans, W., Garcia-Baonza, V., & Lorenzana, H. 1998, JLTP, 111, 247
Luspay-Kuti, A., Mousis, O., Lunine, J. I., et al. 2018, SSRv, 214, 115
Martin, J. M. L., & Taylor, P. R. 1997, AcSpA, 53, 1039
Martín-Doménech, R., Manzano-Santamaría, J., Caro, G. M., et al. 2015, A&A, 584, A14
Meredith, C., Hamilton, T. P., & Schaefer, H. F., III 1992, JPC, 96, 9250
Mills, I. M. 1972, in Molecular Spectroscopy—Modern Research, ed. K. N. Rao & C. W. Mathews (New York: Academic), 115
Moll, N. G., Clutter, D. R., & Thompson, W. E. 1966, JChPh, 45, 4469
Møller, C., & Plesset, M. S. 1934, PhRv, 46, 618
Mousis, O., Ronnet, T., Lunine, J., et al. 2018, ApJ, 858, 66
Papousek, D., & Aliev, M. R. 1982, Molecular Vibration-Rotation Spectra (Amsterdam: Elsevier)
Pierce, D. M., & A'Hearn, M. F. 2010, ApJ, 718, 340
Radhakrishnan, S., Gudipati, M. S., Sander, W., & Lignell, A. 2018, ApJ, 864, 151
Raghavachari, K., Trucks, G. W., Pople, J. A., & Head-Gordon, M. 1989, CPL, 157, 479
Rothman, L. S., Hawkins, R. L., Wattson, R. B., & Gamache, R. R. 1992, JQSRT, 48, 537
Shimanouchi, T. 1972, Tables of Molecular Vibrational Frequencies, Vol. 1 (39th ed.; Washington, DC: National Standards Reference Data System)
Taquet, V., Furuya, K., Walsh, C., & van Dishoeck, E. F. 2016, MNRAS, 462, S99
Theis, R. A., & Fortenberry, R. C. 2016, MolAs, 2, 18
Wagner, J. P., McDonald, D. C., II, & Duncan, M. A. 2018, Angew. Chem. Int. Ed., 57, 5081
Watson, J. K. G. 1977, in Vibrational Spectra and Structure, ed. J. R. During (Amsterdam: Elsevier), 1
Werner, H.-J., Knowles, P. J., Knizia, G., Manby, F. R., & Schütz, M. 2012, WIREs Comput. Mol. Sci, 2, 242
Werner, H.-J., Knowles, P. J., Knizia, G., et al. 2015, MOLPRO, Version 2015.1, a Package of ab Initio Programs, http://www.molpro.net
Xie, Y., Allen, W. D., Yamaguchi, Y., & Schaefer, H. F., III 1996, JChPh, 104, 7615
Yao, Y., & Giapis, K. P. 2017, NatCo, 8, 15298
Yu, Q., Bowman, J. M., Fortenberry, R. C., et al. 2015, JPCA, 119, 11623
Zhao, D., Doney, K. D., & Linnartz, H. 2014, ApJL, 791, L28
Zheng, W., Jewitt, D., & Kaiser, R. I. 2006, ApJ, 639, 534